nature biomedical engineering

Article

https://doi.org/10.1038/s41551-025-01604-4

Symbiotic transcatheter pacemaker for lifelong energy regeneration and therapeutic function in porcine disease model

Received: 27 July 2023

Accepted: 10 December 2025

Published online: 19 January 2026

Check for updates

Han Ouyang[1,2,3,12], Dongjie Jiang[1,4,12], Yiran Hu[5,6,12], Sijing Cheng[5,12], Zhengmin Zhang[7,12], Bojing Shi[8], Engui Wang[1], Jiangtao Xue[2], Yizhu Shan[3], Lingling Xu[1], Yang Zou[2,9], Sixian Weng[5], Hui Li[10], Hongxia Niu[5], Min Gu[5], Lin Luo[1], Shengyu Chao[3], Puchuan Tan[3], Yan Yao[11], Ningning Wang[7], Yubo Fan[8], Zhong Lin Wang[1,3], Wei Hua[5] ✉ & Zhou Li[2,9] ✉

Lifelong pacing is one of the ultimate goals of cardiac pacemakers. However, meeting the critical energy condition for lifelong service is a tremendous challenge. Here we report a symbiotic transcatheter pacemaker that regenerates electric energy from heart motion via electromagnetic induction and surpasses the critical energy condition for lifelong service. The pacemaker can be closely integrated with the body owing to favourable biocompatibility and hemocompatibility, and its small size enables interventional delivery. To minimize energy loss and eliminate mechanical collision and friction, we propose a straightforward magnetic levitation energy cache structure. The energy regeneration module has a near-zero boot threshold, high kinetic energy conversion efficiency and intracardiac root mean square output power. We show the energy regeneration and therapeutic function of the symbiotic transcatheter pacemaker over a month-long autonomous operation in a porcine model of brady-arrhythmia. These advances may provide a potential path to extend the service life of pacemakers to the level of the natural heart.

Pacemakers support millions of lives and represent one of the most important inventions in human history, having evolved from being percutaneous, wearable and implantable to being intracardiac transcatheter devices underpinned by innovations in power sources and electronics[1–4]. The transcatheter pacemaker launched in 2016 represents a milestone in the development of cardiac pacemaker technology[3,4]. The tiny size of the transcatheter pacemaker allows it to be closely integrated with the body, similar to natural organs. However, its service life expectancy (8–10 years) is well below that of the natural organ level owing to power source limitations[5]. Fortunately, the service life of the pacemaker is expected to prolong by regenerating electricity from metabolic and other activities of the body[6–8]. This type of pacemaker can even maintain a symbiotic relationship with the body to extend its service life[9]. Lifelong operation is achievable if the critical energy condition for lifelong service is met, in which the device regenerates more energy than it consumes (Supplementary Note 1). The heart has sufficient mechanical energy (1.4 W) compared with the energy requirements of the pacemaker (10 μW)[10]. According to calculations, approximately 400–800 μJ of mechanical energy per heartbeat can be used to generate electricity (Supplementary Note 2).

In recent years, mechanical energy harvesting technology has attracted extensive attention[11–15]. Various energy harvesting techniques, such as electromagnetic generators[16–23], piezoelectric nanogenerators[24–39] and triboelectric nanogenerators[9,40–47], have been developed to regenerate electrical energy from living organisms for powering implantable devices. Triboelectric and

A full list of affiliations appears at the end of the paper. ✉e-mail: drhuawei@fuwai.com; li_zhou@tsinghua.edu.cn

https://doi.org/10.1038/s41551-025-01604-4

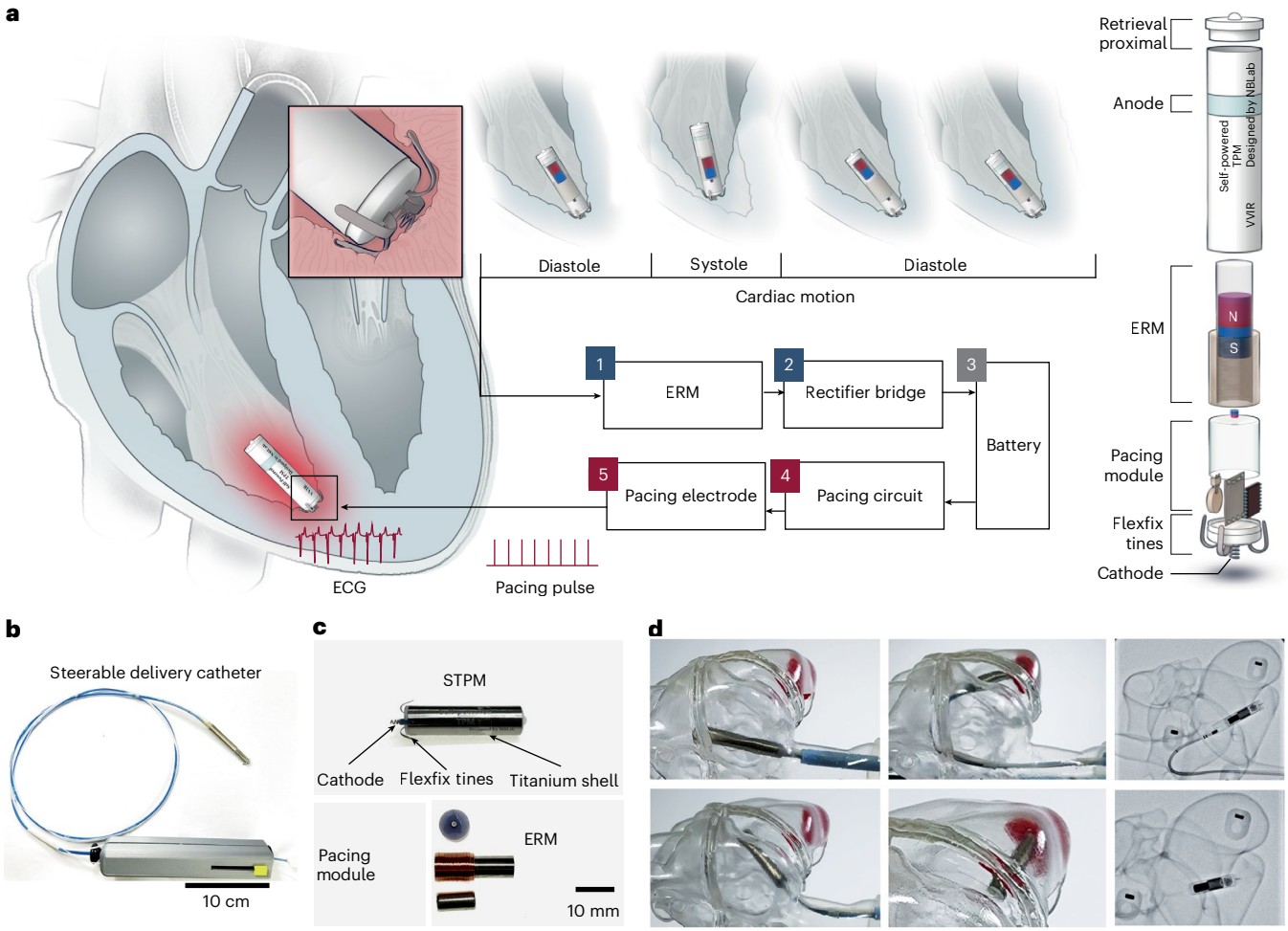

Fig. 1 | Overview of the STPM. a, Schematic structure diagram and work principal diagram of STPM. **b**,**c**, Optical image of the steerable delivery catheter (**b**) and STPM (**c**). **d**, Demonstration of the simulated delivery process of the STPM.

piezoelectric devices exhibit advantages in voltage output[9,33,43]. But it is difficult for these tiny devices to sustainably power a pacemaker owing to limitations in average power and energy conversion efficiency. Electromagnetic power generation devices are strong candidates because of their high conversion efficiency and stability. Some cardiovascular devices based on electromagnetic effects have been approved by the Food and Drug Administration, such as implantable ventricular assist devices[48]. It has shown excellent safety and stability of electromagnetic devices in clinical practice. In addition, some power generation devices based on electromagnetic effects have a lifespan of decades[49].

It remains challenging to harvest energy efficiently from discontinuous cardiac motion with a short time, low frequency and small displacement through an imperceptible process that does not affect the heart's state. In addition, most self-powered pacing devices having separate energy harvesting and pacing modules. Previous efforts are not usually compatible with clinical guidelines, bringing additional surgical risks and trauma, and thus offering low benefit for patients owing to the above limitations.

Here we propose a symbiotic system by regenerating electrical energy from the organism's motion to extend the service life of the implanted electronic device towards that of the natural organ level. We report a symbiotic transcatheter pacemaker (STPM) that can regenerate electric energy from heart motion to maintain its operation (Supplementary Video 1). A total of 11 experimental Yorkshire pigs were used to explore and optimize the design of the STPM, delivery catheter and delivery pathway. The energy regeneration module with a straightforward magnetic levitation energy cache structure can achieve a near-zero boot threshold, high kinetic energy conversion efficiency and sufficient intracardiac output power, where its voltage also reaches 2–2.5 V (3 pigs), meeting the voltage required for pacemakers. The STPM passed 300 million cycles long-term stability (approximately 10 years at a heart rate of 60 bpm), biocompatibility and hemocompatibility tests. In a month-long proof-of-concept trial in large animals, STPM achieved continuous therapeutic function for severe brady-arrhythmia. These results demonstrate the STPM as one of the most promising techniques for next-generation cardiac pacemakers.

Results

Overview of STPM

To complete device implantation by a minimally invasive interventional operation, an all-in-one design is realized. The pacing circuit module, pacing electrodes, energy regeneration and management modules are integrated into one device (Fig. 1a and Supplementary Fig. 1). The energy regeneration module (ERM) is a microlinear generator with a magnetic levitation energy cache structure, which can convert biomechanical energy from cardiac motion into electrical energy. The STPM also integrates a rectifier bridge and battery to store electric energy and power the pacing circuit. A pulsed electric field is formed between the negative and positive electrodes to capture and control heart rhythm. The STPM is anchored in the right ventricle by flex nitinol

hook teeth. The pacing electrode comprises nitinol with a flexible spring structure and a titanium shell partially encapsulated by parylene (Fig. 1b–d).

Evaluation of the ERM

The ERM mainly comprises a movable cylindrical magnet and coil. A small magnet is fixed at the bottom to realize that magnetic levitation of the movable magnet relies on the magnetic field repulsive force to counteract gravity. This moving magnet induces a change in magnetic flux through the coil and generates an induced current. To verify the performance of the ERM, a linear motor was used to simulate cardiac motion. Here the ERM with a 10 mm height movable magnet showed the best voltage (3.5 V), energy output (169 μJ) and energy conversion efficiency (23%) driven by linear motor (acceleration = 10 m s^{-2}, displacement = 8.7 mm) (Fig. 2a and Supplementary Fig. 2a,b). The heartbeat reference acceleration conditions are 6.7 m s^{-2} to 15.8 m s^{-2} (ref. 20). In brief, as the height of the magnet increases, the magnetic flux increases, which lead to an increase in output. Increasing the magnet height further to more than 10 mm causes the output power to decrease owing to the limitations of the movable space that lead the change in magnetic flux to decrease. The approach effectively increased the energy conversion efficiency from 0.0003% at 0.6 V to 24% at 3.5 V through the magnetic levitation energy cache structure design (Fig. 2b and Supplementary Fig. 3a–e). The output of the magnetically levitated structure, designated as ERM, demonstrated an increase with acceleration, reaching a maximum at 14 m s^{-2}, followed by a slight decay at 16 m s^{-2} owing to the limited movable displacement of the magnet. The output voltage was observed to range between 1.8 V and 4.8 V under heartbeat reference acceleration conditions of 6.7 m s^{-2} to 15.8 m s^{-2}, compared with a range of 0.01 V to 0.7 V for the ERM with the non-magnetically levitated structure (acceleration = 2–16 m s^{-2}, displacement = 8.7 mm).

This performance of ERM is also consistent with finite element analysis results (Fig. 2c,d and Supplementary Video 2). Under the simulated heart beating parameters (acceleration = 10 m s^{-2}, displacement = 8.7 mm), the open circuit voltage, short circuit current, energy and energy conversion efficiency reach 3.5 V, 1.5 mA, 175 μJ and 24%, respectively (Fig. 2e,f). The ERM output voltage remains stable at 2.5 V to 3.3 V, with the tilt angle with gravity increasing from 0 to 90 degrees (Fig. 2g). This ensures the power supply capability of the device in different postures (Supplementary Figs. 4a–d and 5).

The effective electric power of the ERM showed that the instantaneous current decreased and voltage rose with increasing load resistance (Fig. 2h). Hence, a peak power of 1.1 mW was achieved at a load resistance of 1,300 Ω (Fig. 2i). The output voltage of ERM remains stable without attenuation in both atmospheric and liquid environments (Fig. 2j). A 100 μF capacitor can be charged to 2 V in 40 s when the simulated heartbeat value is 96 bpm. The device fully meets the power supply requirements of 1.5 V and 3.5 μW (Supplementary Note 3) for the cardiac pacing module (Fig. 2k and Supplementary Fig. 6). Here the ERM can directly charge the lithium-ion battery owing to the large current of the ERM. The charging peaks induced by the ERM charging the lithium-ion battery and the discharging peaks induced by the depletion of the pacing circuit can be clearly observed. The power supply system for the pacemaker module is constantly stable even in the presence of charging and discharging peaks owing to the relatively small peaks and widths of charging and discharging (Supplementary Fig. 7a,b). After an accelerated fatigue test (15 Hz, 8 mm) in phosphate buffer solution (PBS) for 300 million cycles, the output voltage of the ERM was maintained at 6 V (Fig. 2l,m).

Stability and biosafety assessment before in vivo experiment

Before the in vivo study, the entire device and each module were evaluated. The hook tooth structure can be expanded under a thrust force ≥2 N and retracted under a pulling force ≥2.6 N (Supplementary Fig. 8a,b). The anchoring force is ≥1 N (Supplementary Fig. 9a,b). These mechanical data meet the requirements of interventional surgery and postoperative anchoring of the STPM. A steerable delivery catheter was designed to ensure that the STPM could be delivered to the right ventricle across blood vessels and the tricuspid valve (Supplementary Fig. 10). In addition, cell culture and blood compatibility tests confirmed the good biological and blood compatibility of STPM (Extended Data Figs. 1 and 2). The pacing module and electrode function are intact after 231 days and 300 million cycles of immersion in a PBS solution (Supplementary Fig. 11).

Energy regeneration in vivo

A total of 11 experimental Yorkshire pigs (Supplementary Table 1) were used to explore and optimize the design of the delivery catheter (1# and 2# pigs), STPM (3#–9# pigs) and delivery pathway (10# and 11# pigs). STPM is delivered to the right ventricle by a steerable delivery catheter via a 26 Fr sheath (Supplementary Video 3). Then, the STPM was released and anchored in the right ventricular endocardium. The hook teeth and tip of the cathode penetrated the myocardium (Fig. 3a–d, Supplementary Figs. 12 and 13, and Supplementary Video 4).

The maximum open circuit voltage, short circuit current and root mean square (RMS) output power reached 2.5 V, 1.3 mA and 120 μW when the heart motion parameters were 138 bpm and 130/85 mm Hg, respectively. The RMS voltage and RMS current are 0.326 mA and 0.72 V. The ERM can direct light up 50 light-emitting diodes (LEDs) with the electricity regenerated from beating heart (Fig. 3e–g, Supplementary Figs. 14–16 and Supplementary Video 5). The relationship between blood pressure and electrical output was also studied in an animal model with a large blood pressure span. The ERM produced nearly no output when the blood pressure difference was less than 5 mm Hg; then the blood pressure difference showed a linear relationship with the output voltage across the range of 5–45 mm Hg (Fig. 3h and Supplementary Fig. 17). The intercept = −0.298 ± 0.052, slope = 0.055 ± 0.0015 and statistics R^2 = 0.90. Within 100 s, the lithium battery can be charged from 0 V to 1.8 V (Fig. 3i). In the 3 trials in large animals, the output voltage of the ERMs is higher than 2 V, and the current is close to 1 mA (Fig. 3j and Supplementary Figs. 18 and 19). The in vivo electric output of the ERM meets the energy and voltage requirements of the pacing module.

Compared with other energy harvesting devices that can be implanted into the right ventricle, the ERM of the STPM exhibits excellent long-term stability and output power, both of which present an order of magnitude improvement. The RMS output power of 120 μW and the long-term stability of 300 million cycles allow the STPM to meet clinical needs with promising clinical potential (Fig. 3k and Supplementary Table 2). A straightforward magnetic levitation energy cache structure is proposed to eliminate mechanical collision and friction, and avoid energy loss, which allowed a low boot threshold and high kinetic energy conversion efficiency. Compared with other implanted energy harvesting devices, this STPM is a fully implanted device that both meets the critical energy (10 μW) and voltage (1.5 V) condition for pacemakers. Notably, the fully implanted inertia-driven triboelectric nanogenerator[43] with the power density (4.9 μW RMS cm^{-3}) implanted in the back of an adult mongrel also approached this condition. In addition, the lead magnesium niobate lead titanate (PMNPT)-based piezoelectric device with the RMS power (22.4 μW and 58.9 μW) implanted into the pericardial sac of an adult swine (40 kg) facing the cardiac apex also achieved this condition[33,38]. The output power of the STPM is higher than that of the devices implanted between the heart's outer wall and the pericardium through experimental open-heart surgery (Fig. 3l and Supplementary Table 3). Moreover, the STPM is an all-in-one miniaturized intracardiac device that shows superiority in existing interventional surgery clinical guidelines compared with other implanted energy harvester devices.

https://doi.org/10.1038/s41551-025-01604-4

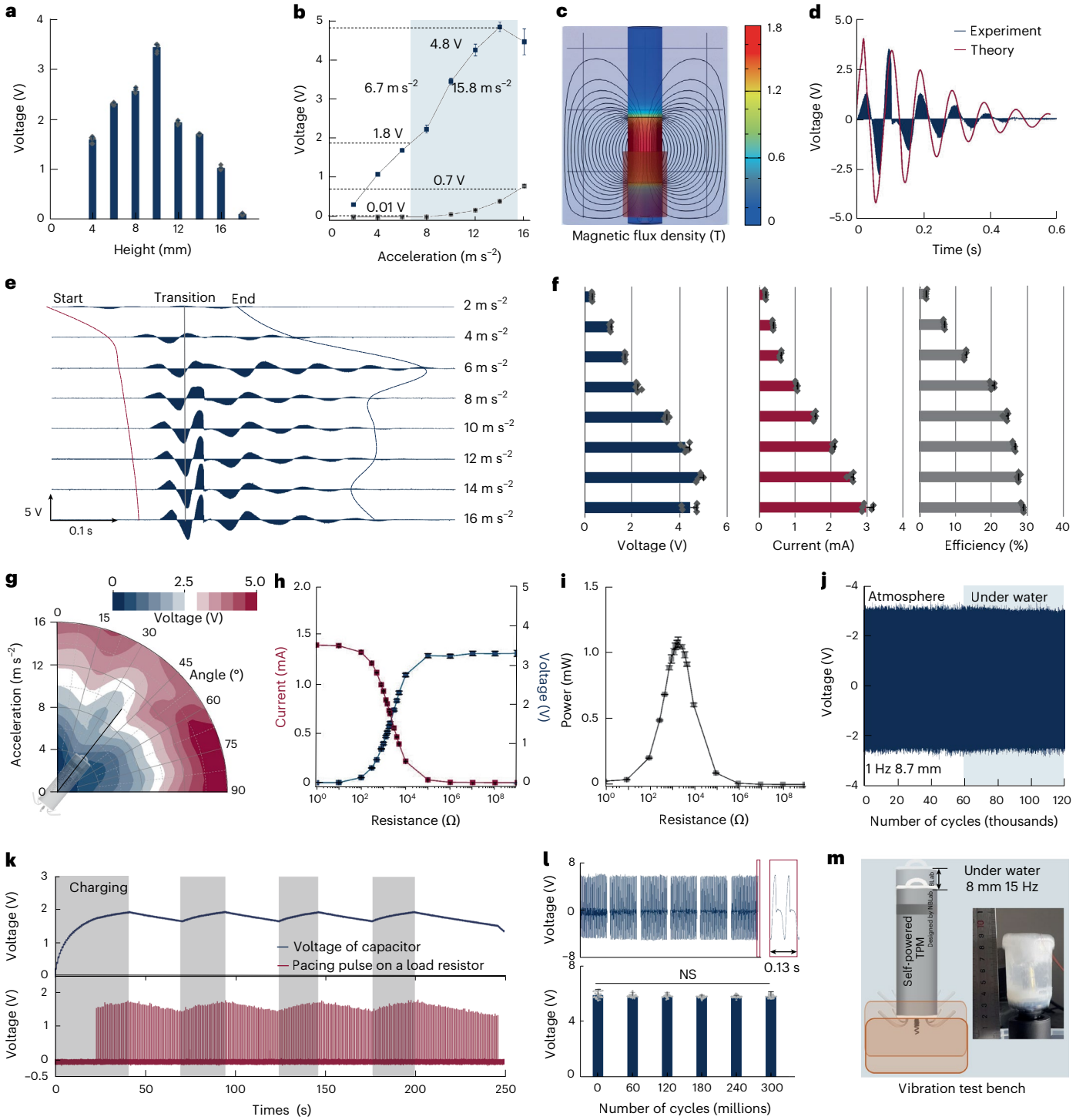

Fig. 2 | Output performance of the energy harvesting module. a, Open circuit voltage of ERM with magnets of different heights. Data are expressed as mean ± s.d. of technical replicates ($n = 6$). **b**, Open circuit voltage of ERM with or without magnetic levitation energy cache structure in different accelerations. Data are expressed as mean ± s.d. of technical replicates ($n = 5$). **c**, Magnetic flux density distribution of ERM. **d**, The theoretical output value is based on finite element analysis and experimental output voltage. **e**, The output voltage of ERM under simulated cardiac motion (acceleration = 2–16 m s^{-2}, displacement = 8.7 mm). **f**, Statistical results of open circuit voltage, short circuit current and energy conversion efficiency under simulated cardiac motion. Data are expressed as mean ± s.d. of technical replicates ($n = 5$). **g**, ERM output voltage at tilt angles with gravity of 0–90 degrees. **h**,**i**, The output voltage, current (**h**) and peak power (**i**) at different load resistances. Data are expressed as mean ± s.d. of technical replicates ($n = 5$). **j**, The output voltage of ERM in atmospheric and liquid environments. **k**, Charging and discharging curve of a 100 µF capacitor charged by ERM and power to pacing module. **l**, The output voltage of ERM under the 300 million cycles accelerated fatigue test (vibration table, displacement = 8 mm, frequency = 15 Hz; approximately 10 years at a heart rate of 60 bpm). NS, no significant difference. Data are expressed as mean ± s.d. of technical replicates ($n = 30$). **m**, Schematic diagram and photograph of the vibration test bench. Source data of **a**, **b**, **f**–**i** and **l** are provided as a Source Data file.

https://doi.org/10.1038/s41551-025-01604-4

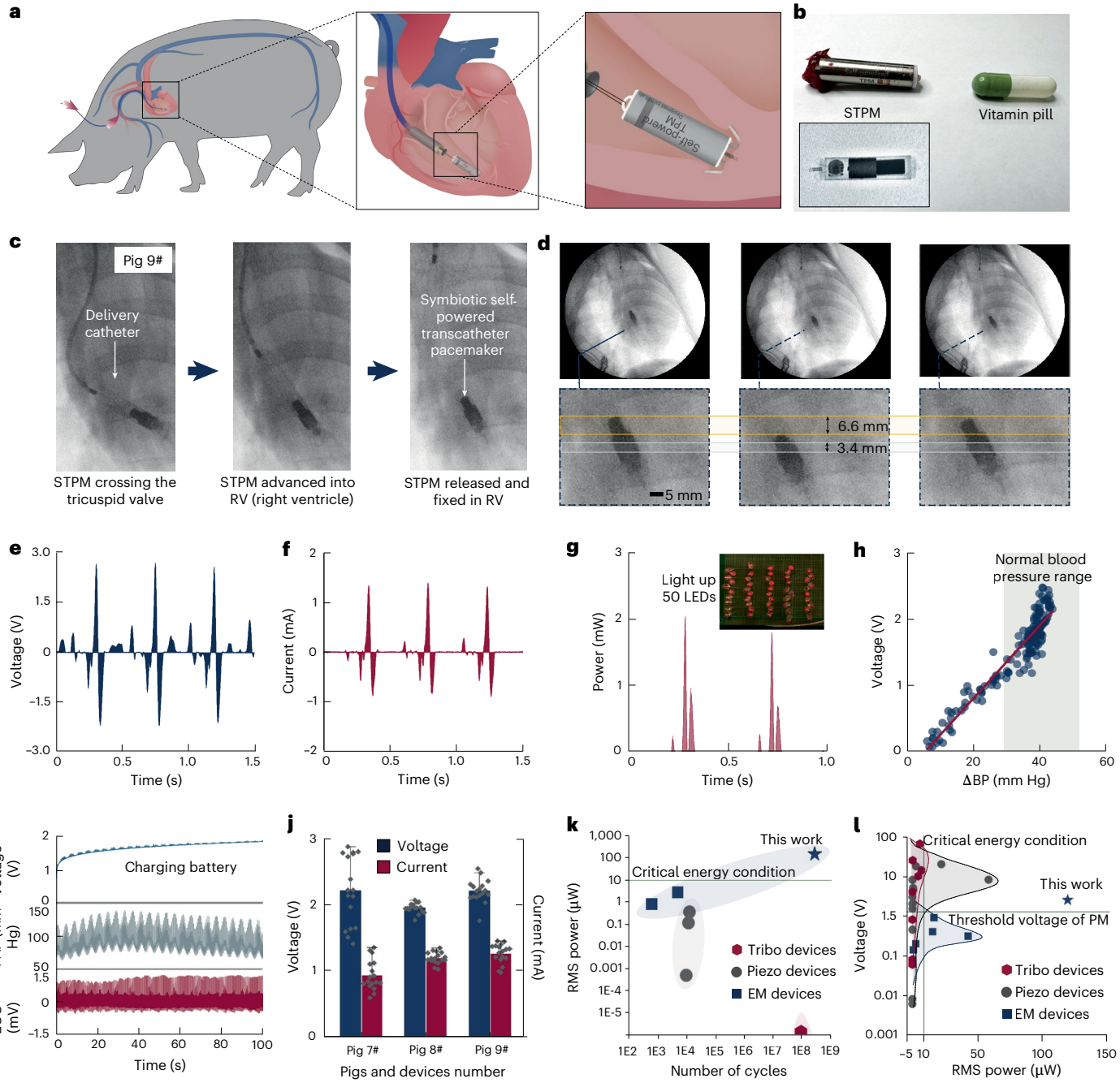

Fig. 3 | In vivo energy harvesting and electrical characterization. a, Diagrams of the STPM implant process. **b**, Optical and digital radiography images of STPM. **c**, STPM implant process in animal experiments. **d**, The movement of the STPM driven by cardiac contractions after anchoring in the right ventricle. **e**–**g**, In vivo experimental electrical characterizations of the open circuit voltage (**e**), short circuit current (**f**) and power (**g**) of ERM. **h**, The linear relationship is fitting between blood pressure difference and output voltage. **i**, ERM charges the lithium battery. **j**, The output voltage of the ERM in three large animal trials. Data are expressed as mean ± s.d. of technical replicates ($n = 17$). **k**, Long-term stability and output power of ERM compared with other energy harvesting devices[16,20,26,28,29,41] that can be implanted into the right ventricle. EM, electromagnetic. **l**, Output voltage and power in vivo of ERM compared with other implanted energy harvesting devices[9,16–47]. PM, pacemaker. Source data of **j** is provided as a Source Data file.

A month-long autonomic operation in large animals

The quality of STPM needs to be checked before implantation, confirming that its pacing pulse meets pacing requirements (Supplementary Fig. 20 and Supplementary Video 6). The entire STPM device and delivery system were fumigated with ethylene oxide. Radiofrequency ablation was used to construct a severe brady-arrhythmia animal model (third-degree atrioventricular block) (Supplementary Fig. 21). Then, the STPM was delivered to the right ventricle via femoral artery access and released and anchored at the right ventricular apex. Postoperative follow-up was performed 1, 14 and 30 days after STPM implantation. Digital radiography images showed that the STPM implantation position remained morphologically intact within 1 month (Fig. 4a).

The heart rate, blood pressure and left ventricular ejection fraction of severe brady-arrhythmia model animals are maintained at 47 bpm, 85/45 mm Hg and less than 45%, respectively, and urgently need effective treatment. After implantation, the STPM is powered by regenerative electrical energy from heart motion and exhibits pacing

https://doi.org/10.1038/s41551-025-01604-4

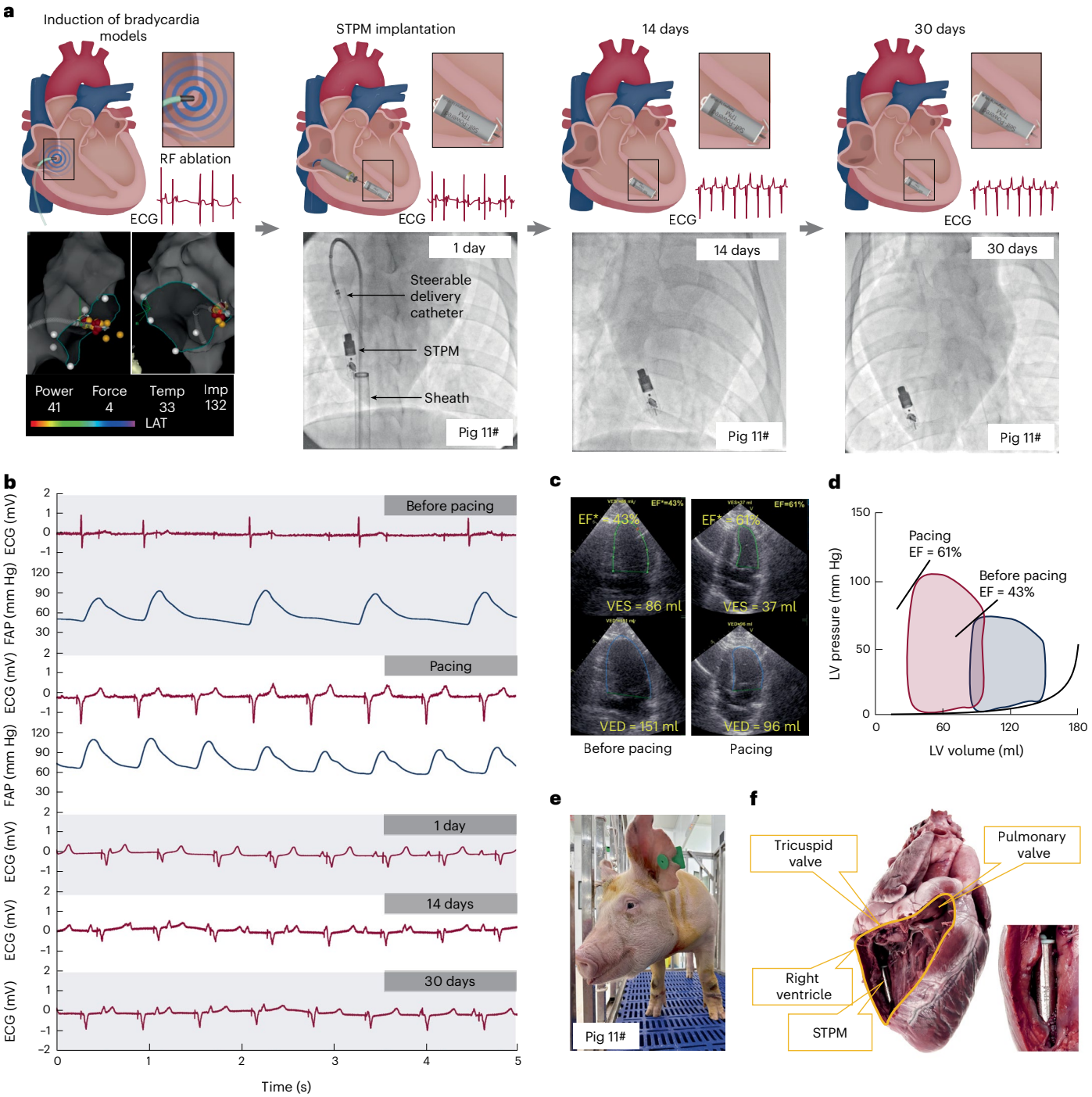

Fig. 4 | Evaluation of therapeutic function on severe brady-arrhythmia in a month-long proof-of-principle trial. a, The design and operation process of the month-long proof-of-principle trial, three-dimensional electrical anatomy of induction of bradycardia models and digital radiography imaging of heart after STPM implantation in 0, 14 and 30 days. **b**, Blood pressure and ECG and postoperative ECG monitoring. **c**, Echocardiography before and after cardiac pacing. EF, ejection fraction; VES, volume of end-systolic; VED, volume of end-diastolic. **d**, Transthoracic echocardiogram and left ventricular volume loop before and after pacing therapy. LV, left ventricle. **e**, Recorded photos of the experimental animal recovery process. **f**, Anatomy results of animal heart samples 1 month after implantation.

and therapeutic functions. The heart rate of experimental animals was raised to the preset 98 bpm, and the blood pressure improved to 110/70 mm Hg (Fig. 4b and Extended Data Fig. 3a,b). The cardiac function measured by transthoracic echocardiogram examination also proved that the cardiac pacing therapy of STPM successfully increased the left ventricular ejection fraction from 43% to 61% (Fig. 4c,d and Supplementary Fig. 22). At 1, 14 and 30 days after STPM implantation, the pacing heart rate of the animals remained at 98 bpm, accompanied by clear pacing spikes. The animal recovered well owing to interventional operation (Fig. 4e, Supplementary Fig. 23 and Supplementary Video 7). STPM showed favourable biocompatibility and safety, which integrate with heart tissue (Fig. 4f). The tissue sections of the implantation site did not exhibit any discernible acute inflammatory reactions, which suggests that STPM shows favourable histocompatibility (Supplementary Fig. 24). Finally, STPM achieved therapeutic function over a month-long proof-of-concept trial.

Discussion

In summary, we report an STPM that can regenerate electric energy from heart motion to maintain continuous operation over a month-long proof-of-concept trial in large animals. The RMS output power (120 μW) of the ERM of STPM in an intracardiac device is sufficient to support the operation of most pacemakers (5–10 μW) with full functional modules currently used in clinical practice. It is a notable advance towards clinical practice, compared with previous work, which mostly involved verifying energy harvesting and cardiac pacing during surgery. The materials used, especially those in contact with tissue and blood, are Food and Drug Administration approved (Supplementary Note 4). The design of the STPM, delivery catheter and delivery pathway have been explored and optimized by large animal experiments with 11 pigs. The shape design, material selection and delivery process of the STPM are compatible with existing interventional surgical guidelines while enabling reduced trauma, shorter surgical time and improved postoperative rehabilitation. This is the demonstration of an energy harvester-powered device that realizes in vivo therapeutic effects comparable to battery-powered devices. The straightforward magnetic levitation energy cache structure is contributed to eliminate mechanical collision and friction and avoid energy loss, which allowed a low boot threshold and high kinetic energy conversion efficiency. The tiny size of ERM integrates into the transcatheter pacemaker with ultra-simple circuits and a minimal number of components. These features contribute to the reliability of the ERM of STPM, which also passed a long-term stability test of 300 million cycles (approximately 10 years at a heart rate of 60 bpm). The output performance can be enhanced by increasing the number of coils and the magnetic remanence of the magnet, as well as optimizing the structure of the ERM module.

There are still some limitations that need to be addressed for clinical practice, including the long-term safety, magnetic interference or MRI compatibility, and functional integration issues. The long-term safety still needs to be supported by more rigorous and comprehensive testing, such as long-term large animal experiments at the year level, and longer in vitro accelerated testing experiments. In addition, magnets potentially interfere with electronic memory and communication components. The risk of interference of magnets in STPM with other electronic components needs to be assessed more thoroughly and comprehensively, although no substantial interference was observed in the current experiments. In the future, other functional modules (communication, sensing and computing modules) will need to be integrated into the STPM, which may increase the size of the pacemaker circuit. For clinical translation, it is important to develop an application-specific integrated circuit chip and embedded code compatible with the energy harvester-powered pacemaker and to further miniaturize the circuit and the STPM. In summary, more careful, detailed and long-term evaluation and optimization are needed before clinical practice. These advances may provide a potential way to extend the service life of pacemakers to the level of the natural heart.

Methods

Fabrication of the ERM

The ERM is a microlinear generator with a magnetic levitation energy cache structure comprising four parts: a linearly movable magnet, a fixed magnet, an inductance coil and a titanium alloy lined tube. The linearly movable magnet is a 5 mm × 10 mm cylindrical neodymium magnet (N52, Ningbo Liyou Magnetic), and the fixed magnet is a small magnet (1.5 mm × 1 mm) (N52, Ningbo Liyou Magnetic). The reference values for the performance of these N52 magnets are as follows: remanence (Br) = 1.45 T, coercivity (Hcb) = 988.3 kA m^{-1} and maximum magnetic energy product (BH) max = 50.31 MGOe. In general, higher coercivity and remanence of the magnet material also result in better output performance of the ERM. The induction coil is made of 40 μm diameter enamelled copper wire wound on a titanium alloy lined tube, approximately 2,300 turns. The titanium alloy lined tube's inner diameter and thickness are 5.5 mm and 0.1 mm, respectively. Its inside and outside surfaces have been polished smoothly. The titanium (TA1)-lined tube is manufactured by Shenzhen Tengfei Precision Hardware using a five-axis computer numerical control machining tool.

Design of the energy storage unit

The energy storage unit is composed of a full-wave rectifier bridge (KMB14F, Microdiode Electronics (Shenzhen)) and a rechargeable lithium battery (ML621, Panasonic Industry).

Design of the pacing circuit unit

The pacing module consists of a microcontroller (MSP430, Texas Instruments) and external resistors and capacitors. Here the preset frequency and pulse width of the pacing pulse are 98 bpm and 0.4 ms, respectively.

Fabrication of Flexfix tines

Flexfix tines are made of nitinol ribands (Dongguan Baohong Metal Material) with a thickness of 0.1 mm and a width of 1 mm. The nitinol ribands are bent after heating and then set by cooling. The STPM can be anchored by this flex nitinol hook teeth (Flexfix tines).

Design of the pacing electrode

The cathode of the pacing electrode is composed of a nitinol spring with a wire diameter of 0.2 mm, a length of 5 mm and an outer diameter of 1 mm. The anode is the exposed part of the titanium shell (1 mm wide ring); the rest is encapsulated by the parylene layer.

Design of the encapsulation structure

The encapsulation structure mainly comprises a titanium shell and a polytetrafluoroethylene (PTFE) plug. The outer diameter of the titanium alloy shell is 7.8 mm, the thickness is 0.1 mm, and the length is 30 mm. The PTFE upper plug is a cylinder with a diameter of 7.6 mm and a thickness of 1 mm, and a 2 mm hemispherical table with holes on both sides is reserved at the top. The hemispherical table is used to assist with device positioning and recycling.

Integration of STPM

The pacing circuit module, pacing electrodes, energy regeneration and management modules are connected in series through a wire and integrated into one device (Supplementary Fig. 25). All units are encapsulated in a titanium shell and PTFE plug with a silicone sealant. The overall mass of the STPM is approximately 4.2 g (Supplementary Table 4).

Fabrication of steerable delivery system

A catheter (The Biosense Webster NAVISTAR Catheter), two PTFE thin tubes (1.0 mm/1.3 mm and 2.0 mm/2.3 mm) and a titanium tube (8.0 mm/8.2 mm inner/outer diameter) were used to make the delivery system. High-tenacity polymer recycling wire and titanium–nickel pushing wire pass through two PTFE tubes to control the release and retrieval of STPM. The hemispherical parts with an outer diameter of 8 mm printed in (three dimensions (3D) have reserved apertures of 2.3 mm, 2.3 mm and 1.3 mm at the top and bottom, respectively. Finally, these parts are aligned and glued together with waterproof glue to integrate a steerable delivery system.

Characterization methods

All scanning electron microscope images were taken by field emission scanning electron microscopy (FEI Nova Nano 450). The voltage, transferred charge and current were measured by an electrometer (Keithley 6517B) and recorded by an oscilloscope (Teledyne LeCroy HD 6104) or data acquisition hardware (Biopac MP150). The force was measured by a force and torque measurement equipment (Mark 10). A linear motor (NTI AG LinMot HS01-37×166) simulates biomechanical movement and

drives the ERM. The preset parameters are operating distance, 8.6 mm; acceleration, 2–16 m s^{-2}; and deceleration, 2–16 m s^{-2}.

Force measurement

The applied force was measured by a dynamometer (MARK-10-M5-2). A nitinol wire fixed on the dynamometer pushed the STPM out of the delivery capsule. The relationship curve of the push displacement and force is recorded. Similarly, the retrieve line was fixed on the dynamometer, the STPM was pulled into the delivery capsule, and the displacement and force were recorded simultaneously.

The stability test and the saturated accelerated fatigue test

A linear motor (NTI AG LinMot HS01-37×166) was used for mechanical stimuli during the stability test. The preset parameters are operating distance, 8.6 mm; acceleration, 10 m s^{-2}; and deceleration, 10 m s^{-2}. The measurement method is described in the 'Characterization methods' section.

The vibration table made by our lab was used as a source of mechanical stimuli for the saturated accelerated fatigue test (operating distance, 8 mm; frequency, 15 Hz). The output voltage was measured every 6×10^8 cycles. The measuring method is described above.

Cell biocompatibility test

Four different materials (parylene, titanium (Ti), titanium–nickel alloy (Ti/Ni) and PTFE film) were fixed into the bottom of 24 wells. All the materials were immersed in 75% ethyl alcohol and in sterile water for more than 60 min each in turn, dried on a sterile operating table and disinfected under ultraviolet light for at least 30 min before use for cell seeding.

The cell line L929 (mouse fibroblast cell line) was used to test the biocompatibility of these materials. The cells were cultured in Dulbecco's modified Eagle's medium (high sugar, Solarbio) supplemented with 1% penicillin/streptomycin (Gibco) and 10% fetal bovine serum (Gibco). The cell cultivation conditions were 37 °C and a 5% CO_2 atmosphere. When the proliferation of L929 cells increased logarithmically, they were digested and seeded on the materials.

The Cell Counting Kit-8 (CCK-8) test could reflect the cell viability through the absorbance of the precipitate produced from live cells through formazan at 450 nm. CCK-8 solution (20 µl) was mixed with 280 µl of cell culture medium for each well. After incubating the cells at 1, 3 and 5 days with CCK-8 solution for 1.5 h at 37 °C, 200 µl of cell culture supernatant was transferred into a 96-well plate. The absorbance of the solution in the 96-well plate was measured at 450 nm with a microplate absorbance assay instrument (Bio-Rad iMark).

We chose a calcein-AM/propidium iodide (PI) double-labelled kit (Solarbio) to test the cell survival condition. The appropriate amount of 10× assay buffer was removed under sterile conditions and diluted 10 times with deionized water to obtain 1× assay buffer. The grown cells at 1, 3 and 5 days were detached from the substrates by using 0.25% trypsin-EDTA (ethylenediaminetetraacetic acid) solution, collected into a centrifuge tube and centrifuged at 450 × *g* for 5 min. After removing the supernatant, the cells were washed twice with 1× assay buffer and centrifuged them at 450 × *g* for 5 min. The cell pellet obtained by centrifugation was resuspended in 1× assay buffer. The dosage for the calcein-AM solution was 1–2 µl and 3–5 µl for the PI solution. After adding a certain amount of calcein-AM solution into the cells, the cells were incubated in the shade for 20–25 min at 37 °C. Then, the cells were stained with PI solution in the dark for 5 min at room temperature. Before observation, the cells were centrifuged to remove the staining solution, washed gently with PBS and resuspended in 3 ml PBS. Finally, the cells were visualized by fluorescence microscopy.

Haemolysis test

To monitor the interaction of different materials with blood erythrocytes, healthy rabbit blood containing EDTA anticoagulant was drawn from marginal ear veins. The samples (Ti, Ti/Ni, PTFE and parylene) were immersed in 1.5 ml centrifuge tubes containing 1 ml of PBS, which was previously incubated at 37 °C for 1 h. Then, 20 µl of red blood cells (RBCs) was added to the tube and incubated with the mixture at 37 °C for 3 h. RBC suspensions treated with PBS and deionized water were used as negative and positive controls, respectively. Then, the sample was removed and centrifuged at 390 × *g* for 5 min. The absorbance of the supernatant was measured at 540 nm on 96-well plates. The percentage of haemolysis was calculated based on the average of the four replicates.

Platelet activation and adhesion test

For the platelet activation studies, the level of the platelet activation marker P-serotonin (CD62P) expressed on the platelet surface was measured in vitro. Whole blood was collected by cardiac puncture in SD rats. Samples were soaked in PBS solution at 37 °C for 24 h to prepare the extract. The extract was incubated with whole blood at room temperature for 30 min in the presence of FITC-CD61 (104305, BioLegend; dilution 1:50) and PE-CD62P antibody (148305, BioLegend; dilution 1:100) (BioLegend). Finally, the cells were analysed by flow cytometry to study the non-specific activation of platelets.

For the in vitro studies of further platelet adhesion, whole blood was centrifuged at 200 × *g* for 15 min to prepare platelet-rich plasma. Then, 0.2 ml platelet-rich plasma was added to different material surfaces (Ti, PTFE and parylene) and incubated at 37 °C. After 1 h, non-adherent platelets were gently removed, and the surfaces were washed three times with PBS. The adherent platelets were fixed in 2.5% glutaraldehyde solution at room temperature for 1 h. They were dehydrated in a gradient ethanol/distilled water mixture (50%, 60%, 70%, 80%, 90% and 100% for 10 min) and air-dried. Samples were sputter coated with gold for observation. The surface of the platelet adhesion sample was observed by a scanning electron microscope. Different locations were randomly selected for counting. The value is expressed as platelet adhesion per square millimetre of the surface.

In vivo study

A total of 11 experimental Yorkshire pigs were used to explore and optimize the design of the delivery catheter (1# and 2# pigs), STPM (3#–9# pigs) and delivery pathway (10# and 11# pigs). All experimental processes were strictly in accordance with the institutional and national guidelines for the care and use of laboratory animals. The study protocol was approved by the State Key Laboratory of Cardiovascular Disease and Fuwai Hospital (ethical approval number 0104-1-4-ZX(X)-23).

Animal preparation

Adult Yorkshire pigs (70–90 kg) fasted for 12 h before surgery. Then, the animals were anaesthetized with propofol (0.5 mg kg^{-1}), intubated and maintained on 1–3% isoflurane with positive-pressure ventilation. The right external jugular vein was routinely exposed, and a guidewire was used to obtain access for STPM implantation. After puncturing the right femoral vein, a short 8 Fr sheath was advanced to obtain access for radiofrequency ablation.

Energy regeneration in vivo test

Three large animal models (70–90 kg Yorkshire pig) were used to evaluate ERM output performance in vivo. STPM was delivered to the right ventricle by a steerable delivery catheter via a 26 Fr sheath (GORE DrySeal Flex Introducer Sheath, DSF2665). Then, the STPM was released and anchored in the right ventricle. The hook teeth and tip of the cathode penetrated the myocardium. A dynamic arterial pressure sensor (SD104) was inserted into the right femoral artery and linked the data acquisition hardware (BIOPAC, MP150) for femoral artery pressure (FAP) measurement. The electrocardiogram (ECG) was recorded by data acquisition hardware. The ERM of STPM was then connected

to a capacitor through a rectifier or connected to the electrometer (Keithley 6517B) to measure the electric output or a LED and recorded by data acquisition hardware (BIOPAC, MP150).

STPM system preparation

The anchoring, power generation and pacing capabilities of the STPM need to be checked before implantation. The STPM is pushed and anchored to a cylindrical block of silicone and then placed in saline solution. Then the airtight container was placed on the vibration table (15 Hz, 8 mm) for 5 min fast self-charging. This energy is expected to support about 5.5 h of pacing or about 33 h of no-load standby operation. STPM meets the criteria for implantation as follows: Structurally intact and not intruded by liquids, the Flexfix tines are not detached from the silicone block, and the pacing pulse can be output to light up the LED. The STPM and delivery system were fumigated in ethylene oxide for 6 h. Finally, before implantation, confirm that the pacing pulse generated by STPM has enough voltage and energy to light up the LED (the luminescence threshold is about 1.7 V), which also means that it is sufficient for cardiac pacing (Supplementary Video 6).

Induction of bradycardia pig models

Radiofrequency ablation induced third-degree atrioventricular block in the swine model. A contact force catheter (Thermocool SmartTouch, Biosense Webster) was introduced into the right femoral vein via the 8 Fr sheath. Three-dimensional electrical anatomy of the right atrium and tricuspid valve annulus (white dot and blue circle) were reconstructed using the CARTO-3 system (Biosense Webster) (Fig. 4a and Supplementary Fig. 20). After mapping a cluster of using near-field His-bundle (HB) potential (orange dot), radiofrequency ablation was performed in power-control mode at 35 W (cold saline irrigation flow rate at 15 ml min^{-1}) with a duration of 120 s in this HB region (red dot). The signs of successful ablation were as follows: (1) the emergence of complete atrioventricular block and (2) the occurrence of the escape rhythm.

STPM implantation in bradycardia swine models

The right femoral vein was dissected and cannulated with a 26 Fr sheath for the introduction. The delivery sheath (GORE DrySeal Flex Introducer Sheath, DSF2665) was then advanced into the right atrium over a guidewire (model RF*GA35153M, Terumo Corporation). Guided by fluoroscopy (General Electric medical system), a delivery catheter integrating the STPM was advanced across the tricuspid valve into the right ventricle. Then, the STPM was delivered into the right ventricular apex. Once the device STPM firmly contacted the right ventricular endocardium, the delivery sheath with the catheter was removed outside the pig's heart. After that, the right femoral vein was sutured.

Echocardiography

Echocardiographic parameters were measured perioperatively using the Vivid E95 ultrasound system (GE Vingmed Ultrasound), including left ventricular end-diastolic volume, left ventricular end-systolic volume and left ventricular ejection fraction (Supplementary Fig. 19). Left ventricular ejection fraction was measured with the modified Simpson method.

Histology

The myocardial tissue was fixed in 4% formalin (Solarbio) and then dehydrated in a series of ethanol and xylene solutions (Solarbio) of different concentrations. The tissue was then routinely embedded in paraffin and sectioned with a microtome to produce 4-μm-thick sections. For the observation of tissue morphology and extracellular matrix, we performed standard procedures for haematoxylin and eosin (Solarbio). Finally, optical images were obtained via a pathological section scanner.

Statistical analysis

Data are expressed as the mean ± s.d. One-way analysis of variance (ANOVA) and two-sample *t*-test were used to compare mean values in groups of samples for all experiments. Error bars were calculated using the mean ± s.d., with a group size $n \geq 3$. All reported *P* values were calculated for groups with ANOVA (one-way ANOVA) using Origin software (v2021b). Reported *P* values for all experiments corresponding to $^*P < 0.05$ were considered significant.

Finite element analysis of ERM based on COMSOL software

The finite element calculation software COMSOL Multiphysics (v5.6) is used to simulate and estimate the output of ERM devices. The model size refers to the actual size of the ERM. The displacement and magnetic field change of the movable magnet after being loaded are calculated.

The magnet material is N52 NdFeB. The conductivity, relative permittivity and recovery permeability are 7.14×10^5 S m^{-1}, 10^{19} and 1.05, respectively. Young's modulus, Poisson's ratio and density are 2.1 GPa, 0.28 and 7850 kg m^{-3}. Both relative permeability and permittivity of air are 1. The initial load is 10^4 Pa. The movable and fixed magnet's residual magnetic flux density is 1.4 T and 1.2 T.

Calculation of the peak power density

Output power was used to evaluate the generator output performance. The following equation can derive the output power:

$$\text{Output power} = I^2R$$

where *I* is the output current and *R* is the internal resistance of the coils.

Calculation of energy conversion efficiency

$$\eta = \frac{E_{\text{out-STPM}}}{E_{\text{in-STPM}}}$$

η is the energy conversion efficiency. $E_{\text{out-STPM}}$ is the energy output by the ERM of STPM. $E_{\text{in-STPM}}$ is the mechanical energy input to the STPM from the outside. $M_{\text{STPM}} = 4.2$ g refers to the mass of the STPM, *a* is the acceleration, and $S = 8.6$ mm × 2 refers to the distance travelled by the device driven by an external force.

$$E_{\text{in}} = M_{\text{STPM}} \times a \times S$$

I is the output current, and $R = 1{,}300\ \Omega$ is the internal resistance of the coils:

$$E_{\text{out}} = \int I^2 R dt$$

Reporting summary

Further information on research design is available in the Nature Portfolio Reporting Summary linked to this article.

Data availability

The main data supporting the findings of this study are available within the Article and its Supplementary Information. Owing to the large file sizes and volume of imaging and raw data, the corresponding raw data supporting the findings of this study are available from the senior authors upon request. The source data underlying Figs. 2a,b,f–i,l, 3j and 4j–k and Extended Data Figs. 1b, 2d–f are provided as a Source Data file that has also been shared via figshare at https://doi.org/10.6084/m9.figshare.30246931 (ref. 50). Source data are provided with this paper.

References

1. Yu, K.-H., Beam, A. L. & Kohane, I. S. Artificial intelligence in healthcare. *Nat. Biomed. Eng.* **2**, 719–731 (2018).

2. Saltzman, W. M. *Biomedical Engineering: Bridging Medicine and Technology* (Cambridge Univ. Press, 2015).
3. Reynolds, D. et al. A leadless intracardiac transcatheter pacing system. *N. Engl. J. Med.* **374**, 533–541 (2016).
4. Tjong, F. V. Y. & Reddy, V. Y. Permanent leadless cardiac pacemaker therapy: a comprehensive review. *Circulation* **135**, 1458–1470 (2017).
5. Della Rocca, D. G., Gianni, C., Di Biase, L., Natale, A. & Al-Ahmad, A. Leadless pacemakers: state of the art and future perspectives. *Card. Electrophysiol. Clin.* **10**, 17–29 (2018).
6. MacVittie, K. et al. From "cyborg" lobsters to a pacemaker powered by implantable biofuel cells. *Energy Environ. Sci.* **6**, 81–86 (2013).
7. Zheng, Q., Tang, Q. Z., Wang, Z. L. & Li, Z. Self-powered cardiovascular electronic devices and systems. *Nat. Rev. Cardiol.* **18**, 7–21 (2021).
8. Dagdeviren, C. The future of bionic dynamos. *Science* **354**, 1109 (2016).
9. Ouyang, H. et al. Symbiotic cardiac pacemaker. *Nat. Commun.* **10**, 1821 (2019).
10. Pfenniger, A., Jonsson, M., Zurbuchen, A., Koch, V. M. & Vogel, R. Energy harvesting from the cardiovascular system, or how to get a little help from yourself. *Ann. Biomed. Eng.* **41**, 2248–2263 (2013).
11. Hinchet, R. et al. Transcutaneous ultrasound energy harvesting using capacitive triboelectric technology. *Science* **365**, 491–494 (2019).
12. Chen, G. R., Li, Y. Z., Bick, M. & Chen, J. Smart textiles for electricity generation. *Chem. Rev.* **120**, 3668–3720 (2020).
13. Shepertycky, M., Burton, S., Dickson, A., Liu, Y. F. & Li, Q. G. Removing energy with an exoskeleton reduces the metabolic cost of walking. *Science* **372**, 957–960 (2021).
14. Dagdeviren, C., Li, Z. & Wang, Z. L. Energy harvesting from the animal/human body for self-powered electronics. *Annu. Rev. Biomed. Eng.* **19**, 85–108 (2017).
15. Fernandez, S. V. et al. On-body piezoelectric energy harvesters through innovative designs and conformable structures. *ACS Biomater. Sci. Eng.* **9**, 2070–2086 (2023).
16. Franzina, N. et al. A miniaturized endocardial electromagnetic energy harvester for leadless cardiac pacemakers. *PLoS ONE* **15**, e0239667 (2020).
17. Goto, H., Sugiura, T., Harada, Y. & Kazui, T. Feasibility of using the automatic generating system for quartz watches as a leadless pacemaker power source. *Med. Biol. Eng. Comput.* **37**, 377–380 (1999).
18. Haeberlin, A. et al. Intracardiac turbines suitable for catheter-based implantation—an approach to power battery and leadless cardiac pacemakers? *IEEE Trans. Biomed. Eng.* **67**, 1159–1166 (2020).
19. Tholl, M. V. et al. An intracardiac flow based electromagnetic energy harvesting mechanism for cardiac pacing. *IEEE Trans. Biomed. Eng.* **66**, 530–538 (2019).
20. Zurbuchen, A. et al. Endocardial energy harvesting by electromagnetic induction. *IEEE Trans. Biomed. Eng.* **65**, 424–430 (2018).
21. Zurbuchen, A. et al. The Swiss approach for a heartbeat-driven lead- and batteryless pacemaker. *Heart Rhythm* **14**, 294–299 (2017).
22. Zurbuchen, A. et al. Towards batteryless cardiac implantable electronic devices—the Swiss way. *IEEE Trans. Biomed. Circuits Syst.* **11**, 78–86 (2017).
23. Zurbuchen, A. et al. Energy harvesting from the beating heart by a mass imbalance oscillation generator. *Ann. Biomed. Eng.* **41**, 131–141 (2013).
24. Cheng, X. L. et al. Implantable and self-powered blood pressure monitoring based on a piezoelectric thinfilm: simulated, in vitro and in vivo studies. *Nano Energy* **22**, 453–460 (2016).
25. Dagdeviren, C. et al. Conformal piezoelectric energy harvesting and storage from motions of the heart, lung, and diaphragm. *Proc. Natl Acad. Sci. USA* **111**, 1927–1932 (2014).
26. Dong, L. et al. Multifunctional pacemaker lead for cardiac energy harvesting and pressure sensing. *Adv. Healthc. Mater.* **9**, e2000053 (2020).
27. Azimi, S. et al. Self-powered cardiac pacemaker by piezoelectric polymer nanogenerator implant. *Nano Energy* **83**, 105781 (2021).
28. Dong, L. et al. In vivo cardiac power generation enabled by an integrated helical piezoelectric pacemaker lead. *Nano Energy* **66**, 104085 (2019).
29. Dong, L. et al. Piezoelectric buckled beam array on a pacemaker lead for energy harvesting. *Adv. Mater. Technol.* **4**, 1800335 (2019).
30. Jeong, C. K. et al. Comprehensive biocompatibility of nontoxic and high-output flexible energy harvester using lead-free piezoceramic thin film. *APL Mater.* **5**, 074102 (2017).
31. Kim, D. H. et al. In vivo self-powered wireless transmission using biocompatible flexible energy harvesters. *Adv. Funct. Mater.* **27**, 1700341 (2017).
32. Li, H. D. et al. An implantable biomechanical energy harvester for animal monitoring devices. *Nano Energy* **98**, 107290 (2022).
33. Li, N. et al. Direct powering a real cardiac pacemaker by natural energy of a heartbeat. *ACS Nano* **13**, 2822–2830 (2019).
34. Li, Z., Zhu, G. A., Yang, R. S., Wang, A. C. & Wang, Z. L. Muscle-driven in vivo nanogenerator. *Adv. Mater.* **22**, 2534–2537 (2010).
35. Lu, B. W. et al. Ultra-flexible piezoelectric devices integrated with heart to harvest the biomechanical energy. *Sci. Rep.* **5**, 16065 (2015).
36. Sun, R. J. et al. Stretchable piezoelectric sensing systems for self-powered and wireless health monitoring. *Adv. Mater. Technol.* **4**, 1900100 (2019).
37. Wang, A. C. et al. Piezoelectric nanofibrous scaffolds as in vivo energy harvesters for modifying fibroblast alignment and proliferation in wound healing. *Nano Energy* **43**, 63–71 (2018).
38. Yi, Z. R. et al. A battery- and leadless heart-worn pacemaker strategy. *Adv. Funct. Mater.* **30**, 2000477 (2020).
39. Zhang, Y. Z. et al. Self-powered pacemaker based on all-in-one flexible piezoelectric nanogenerator. *Nano Energy* **99**, 107420 (2022).
40. Li, J. et al. Implanted battery-free direct-current micro-power supply from in vivo breath energy harvesting. *ACS Appl. Mater. Interfaces* **10**, 42030–42038 (2018).
41. Liu, Z. et al. Transcatheter self-powered ultrasensitive endocardial pressure sensor. *Adv. Funct. Mater.* **29**, 1807560 (2019).
42. Ma, Y. et al. Self-powered, one-stop, and multifunctional implantable triboelectric active sensor for real-time biomedical monitoring. *Nano Lett.* **16**, 6042–6051 (2016).
43. Ryu, H. et al. Self-rechargeable cardiac pacemaker system with triboelectric nanogenerators. *Nat. Commun.* **12**, 4374 (2021).
44. Shi, B. J. et al. Body-integrated self-powered system for wearable and implantable applications. *ACS Nano* **13**, 6017–6024 (2019).
45. Yao, G. et al. Effective weight control via an implanted self-powered vagus nerve stimulation device. *Nat. Commun.* **9**, 5349 (2018).
46. Zheng, Q. et al. In vivo powering of pacemaker by breathing-driven implanted triboelectric nanogenerator. *Adv. Mater.* **26**, 5851–5856 (2014).
47. Zheng, Q. et al. In vivo self-powered wireless cardiac monitoring via implantable triboelectric nanogenerator. *ACS Nano* **10**, 6510–6518 (2016).

48. Varshney, A. S. et al. Trends and outcomes of left ventricular assist device therapy. *J. Am. Coll. Cardiol.* **79**, 1092–1107 (2022).
49. Hoseinzadeh, S., Ghasemi, M. H. & Heyns, S. Application of hybrid systems in solution of low power generation at hot seasons for micro hydro systems. *Renew. Energy* **160**, 323–332 (2020).
50. Han, O. et al. Source Data for nBME1980D. *figshare* https://doi.org/10.6084/m9.figshare.30246931.v1 (2025).

Acknowledgements

This project is supported by the National Natural Science Foundation of China grants T2125003 (to Z.L.), 52373256 (to H.O.), 62404011 (D.J.) and 82100325 (to Y.H.); the Beijing Natural Science Foundation Z240022 (to Z.L.) and 7232347 (to H.O.); the National Key Research and Development Program of China grant 2023YFC2411901 (to H.O.); the Beijing Xin Xi Disruptive Technology Innovation Foundation grant 2021005 (to Z.L.); the Beijing Nova Program grant 2024047 (to H.O.); the Youth Innovation Promotion Association CAS grant 2023176 (to H.O.); the Beijing Gold-Bridge Project grant ZZ21055 (to Y.H.); and the Fundamental Research Funds for the Central Universities. This work was completed especially for the 10th anniversary of Nanoenergy and Biosystem Lab. We appreciate the members of the State Key Laboratory of Cardiovascular Disease of the China Research Facility for their help in animal experiment surgery and postoperative care and the members of the BINN and UCAS research facilities for their help in microfabrication/characterization. We are grateful to X. Qu, X. Wang (SICNU) and other laboratory members for their cooperation and advice in this study.

Author contributions

Z.L. and H.O. conceived and coordinated the project and experiments. D.J., W.H., B.S., Y.H., S.C. and Z.Z. assisted in concept development, sample preparation and paper writing. H.O. and D.J. prepared ERM and STPM and collected data in all experiments. L.X., Y.S. and E.W. conducted the stability and biosafety assessments. J.X. assisted in the finite element analysis. H.O., D.J. and Z.Z. conducted the pacing circuit design. W.H. directed, and Y.H., S.C., S.W., H.L., H.N. and M.G. conducted the in vivo animal experiments and month-long proof-of-principle trial. D.J. and H.O. prepared all other samples, conducted all other experiments and wrote the paper. Z.L., W.H. and H.O. directed the project. All authors read and revised the paper.

Competing interests

The authors declare no competing interests.

Additional information

Extended data is available for this paper at https://doi.org/10.1038/s41551-025-01604-4.

Supplementary information The online version contains supplementary material available at https://doi.org/10.1038/s41551-025-01604-4.

Correspondence and requests for materials should be addressed to Wei Hua or Zhou Li.

Peer review information *Nature Biomedical Engineering* thanks Sang-Woo Kim, Jai-Wun Park and Panos E. Vardas for their contribution to the peer review of this work. Peer reviewer reports are available.

Reprints and permissions information is available at www.nature.com/reprints.

Publisher's note Springer Nature remains neutral with regard to jurisdictional claims in published maps and institutional affiliations.

[1]School of Nanoscience and Engineering, University of Chinese Academy of Sciences, Beijing, China. [2]Beijing Tsinghua Changgung Hospital, School of Clinical Medicine, Tsinghua University, Beijing, China. [3]Beijing Institute of Nanoenergy and Nanosystems, Chinese Academy of Sciences, Beijing, China. [4]Department of Sports Medicine, Peking University Third Hospital, Institute of Sports Medicine of Peking University, Beijing, China. [5]Department of Cardiology, The Cardiac Arrhythmia Center, State Key Laboratory of Cardiovascular Disease, National Clinical Research Center of Cardiovascular Diseases, Fuwai Hospital, National Center for Cardiovascular Diseases, Chinese Academy of Medical Sciences and Peking Union Medical College, Beijing, China. [6]Department of Cardiology and Macrovascular Disease, Beijing Tiantan Hospital, Capital Medical University, Beijing, China. [7]Hangzhou Dianzi University, Hangzhou, China. [8]Key Laboratory for Biomechanics and Mechanobiology of Chinese Education Ministry, Beijing Advanced Innovation Centre for Biomedical Engineering, School of Biological Science and Medical Engineering, Beihang University, Beijing, China. [9]School of Biomedical Engineering, Tsinghua University, Beijing, China. [10]Department of Ultrasound, State Key Laboratory of Cardiovascular Disease, National Clinical Research Center of Cardiovascular Diseases, Fuwai Hospital, National Center for Cardiovascular Diseases, Chinese Academy of Medical Sciences and Peking Union Medical College, Beijing, China. [11]Department of Cardiology, Being Anzhen Hospital, Capital Medical University, Beijing, China. [12]These authors contributed equally: Han Ouyang, Dongjie Jiang, Yiran Hu, Sijing Cheng, Zhengmin Zhang. ✉e-mail: drhuawei@fuwai.com; li_zhou@tsinghua.edu.cn

https://doi.org/10.1038/s41551-025-01604-4

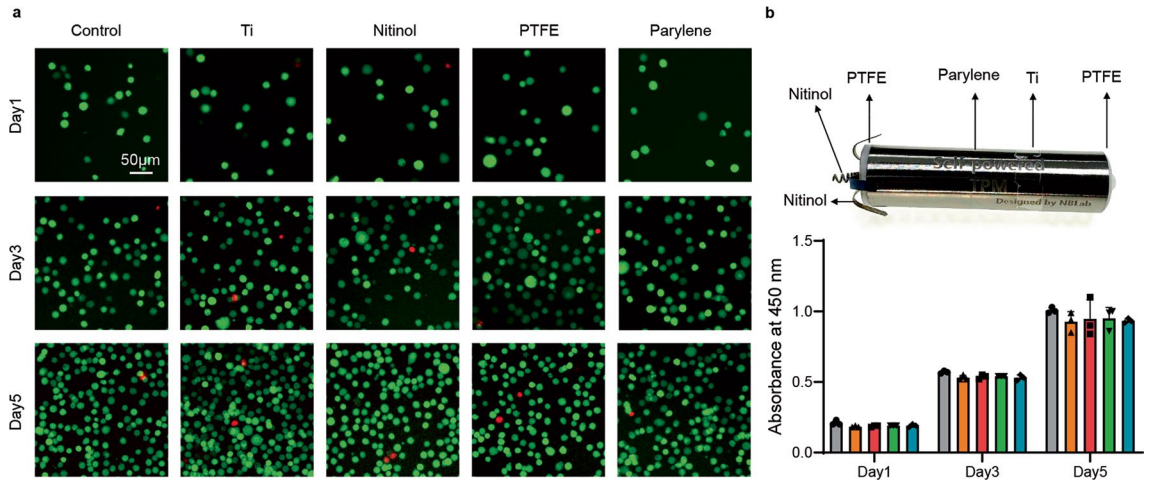

Extended Data Fig. 1 | Cell culture and biological compatibility test. a, Live/Dead stain of cells cultured on cell culture plate, Ti, Nitinol, PTFE and parylene at 1, 3 and 5 days. **b**, The materials used for this device and the CCK-8 results of the absorbance at 450 nm. For all panels, Data are expressed as mean ± s.d. of technical replicates (n = 3). Source data of Extended Data Fig. 1b is provided as a Source Data file.

https://doi.org/10.1038/s41551-025-01604-4

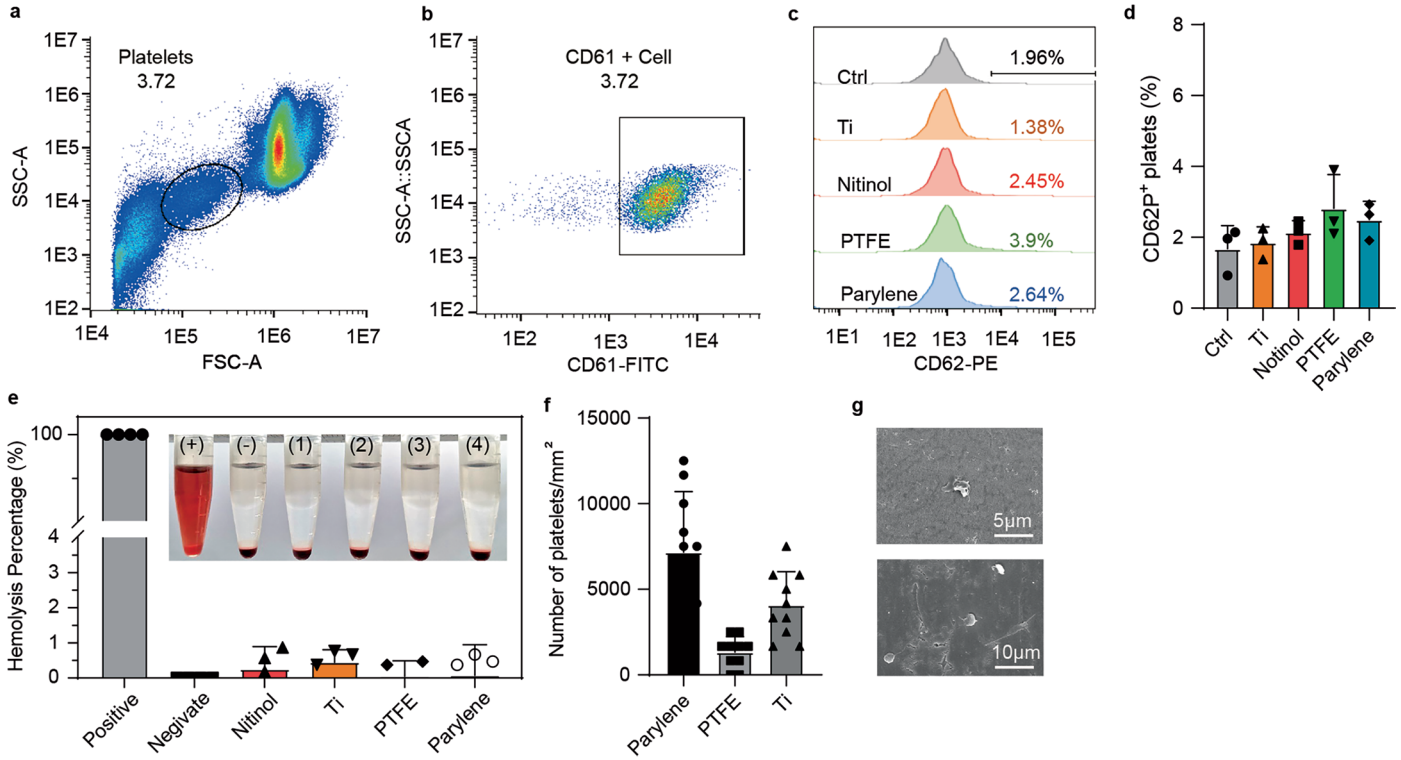

Extended Data Fig. 2 | Flow cytometry analysis of the anticoagulant properties of various materials. a, The forward and side-scattering density plots show that the platelet populations can be distinguished according to the respective light scattering patterns. **b**, Platelets were specifically separated by anti-CD61 monoclonal antibody staining. **c**, The CD61+ platelets were further analyzed for markers of platelet activation using an antibody against CD62P, both of which showed no increase compared to the control. **d**, CD62+ platelets are indicated in each histogram. Data are expressed as mean ± s.d. of technical replicates (n = 3). **e**, Hemolytic assay data of various materials. Hemolytic percentage (%) of RBCs after treatment with different materials at 37 °C for 3 h and corresponding photograph Data are expressed as mean ± s.d. of technical replicates (n = 4). **f**, **g**, Electron microscopy images of platelet adhesion on different materials. Data are expressed as mean ± s.d. of technical replicates (n = 10). Source data of Extended Data Fig. 2d - f is provided as a Source Data file.

https://doi.org/10.1038/s41551-025-01604-4

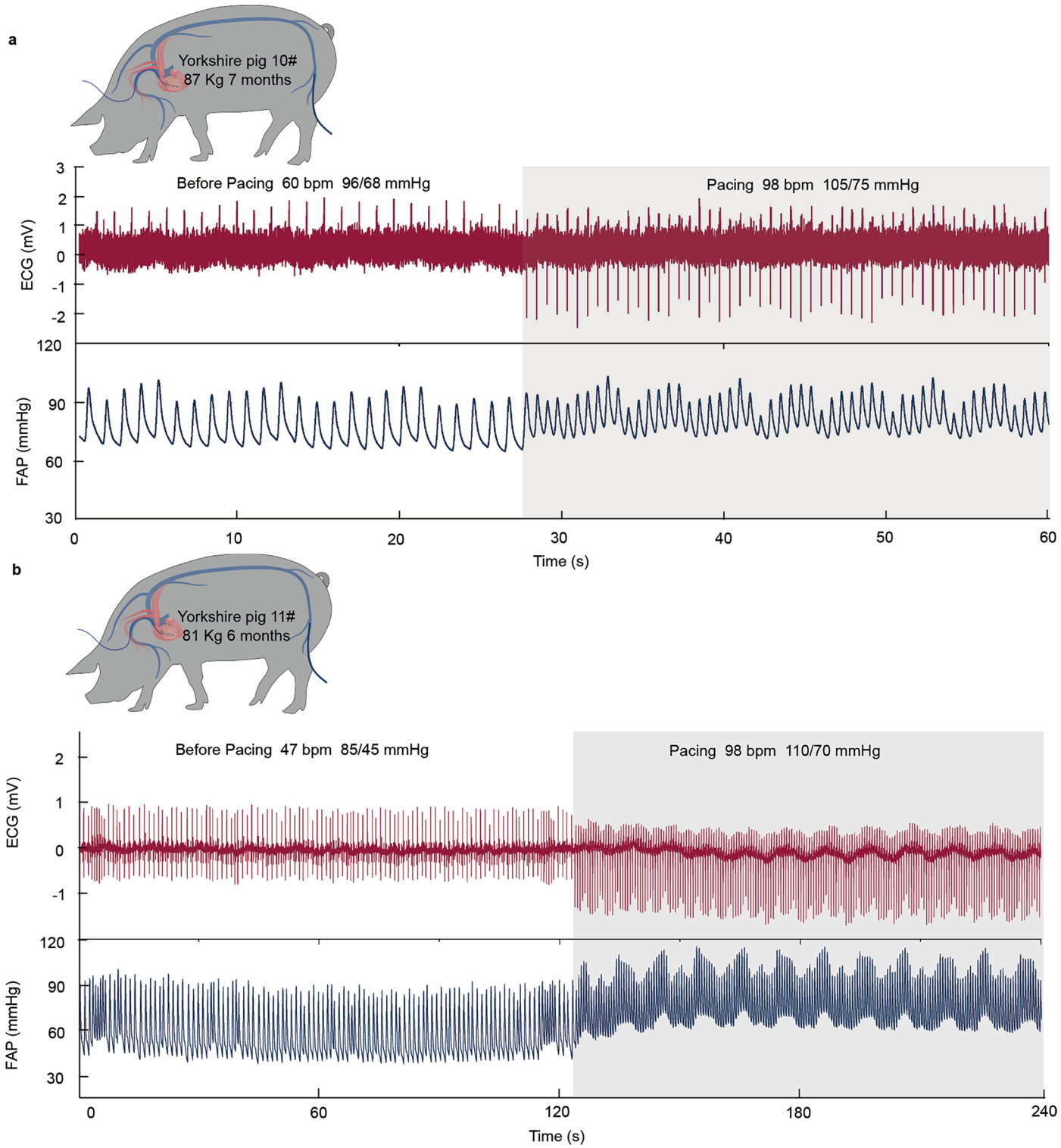

Extended Data Fig. 3 | Blood pressure and ECG monitoring. a, **b**, ECG and FAP after STPM implantation and exhibits pacing therapeutic functions. The heart rate of the experimental animals was raised to the preset 98 bpm, and the blood pressure improved to 110/70 mmHg.

nature portfolio

Corresponding author(s): Zhou Li and Wei Hua

Last updated by author(s): Oct 1, 2025

Reporting Summary

Nature Portfolio wishes to improve the reproducibility of the work that we publish. This form provides structure for consistency and transparency in reporting. For further information on Nature Portfolio policies, see our Editorial Policies and the Editorial Policy Checklist.

Statistics

For all statistical analyses, confirm that the following items are present in the figure legend, table legend, main text, or Methods section.

n/a	Confirmed	
☐	☒	The exact sample size (*n*) for each experimental group/condition, given as a discrete number and unit of measurement
☐	☒	A statement on whether measurements were taken from distinct samples or whether the same sample was measured repeatedly
☐	☒	The statistical test(s) used AND whether they are one- or two-sided *Only common tests should be described solely by name; describe more complex techniques in the Methods section.*
☐	☒	A description of all covariates tested
☐	☒	A description of any assumptions or corrections, such as tests of normality and adjustment for multiple comparisons
☐	☒	A full description of the statistical parameters including central tendency (e.g. means) or other basic estimates (e.g. regression coefficient) AND variation (e.g. standard deviation) or associated estimates of uncertainty (e.g. confidence intervals)
☐	☒	For null hypothesis testing, the test statistic (e.g. *F*, *t*, *r*) with confidence intervals, effect sizes, degrees of freedom and *P* value noted *Give P values as exact values whenever suitable.*
☒	☐	For Bayesian analysis, information on the choice of priors and Markov chain Monte Carlo settings
☒	☐	For hierarchical and complex designs, identification of the appropriate level for tests and full reporting of outcomes
☒	☐	Estimates of effect sizes (e.g. Cohen's *d*, Pearson's *r*), indicating how they were calculated

Our web collection on statistics for biologists contains articles on many of the points above.

Software and code

Policy information about availability of computer code

Data collection	No commercial, open source nor custom code used for data collection.
Data analysis	OriginPro and Excel was used for data analysis and plotting.

For manuscripts utilizing custom algorithms or software that are central to the research but not yet described in published literature, software must be made available to editors and reviewers. We strongly encourage code deposition in a community repository (e.g. GitHub). See the Nature Portfolio guidelines for submitting code & software for further information.

Data

Policy information about availability of data

All manuscripts must include a data availability statement. This statement should provide the following information, where applicable:

- Accession codes, unique identifiers, or web links for publicly available datasets
- A description of any restrictions on data availability
- For clinical datasets or third party data, please ensure that the statement adheres to our policy

The main data supporting the findings of this study are available within the Article and its Supplementary Information. Owing to the large file sizes and volume of imaging and raw data, the corresponding raw data supporting the findings of this study are available from the senior authors upon request. The source data underlying Figs. 2a, b, f-i, l, 3j, and 4j–k and Extended Data Fig. 2b, 3c-e, 4c-d, 10b, 11d are provided as a Source Data that has also been shared on figshare DOI.10.6084/m9.figshare.30246931.

Research involving human participants, their data, or biological material

Policy information about studies with human participants or human data. See also policy information about sex, gender (identity/presentation), and sexual orientation and race, ethnicity and racism.

Reporting on sex and gender	n/a
Reporting on race, ethnicity, or other socially relevant groupings	n/a
Population characteristics	n/a
Recruitment	n/a
Ethics oversight	n/a

Note that full information on the approval of the study protocol must also be provided in the manuscript.

Field-specific reporting

Please select the one below that is the best fit for your research. If you are not sure, read the appropriate sections before making your selection.

☒ Life sciences ☐ Behavioural & social sciences ☐ Ecological, evolutionary & environmental sciences

For a reference copy of the document with all sections, see nature.com/documents/nr-reporting-summary-flat.pdf

Life sciences study design

All studies must disclose on these points even when the disclosure is negative.

Sample size	Two pigs were used for the verification of the cardiac pacemaker, and three pigs were used for the in vivo energy harvesting tests, with the remaining animals allocated to preliminary exploratory studies.
Data exclusions	No data was excluded from the analysis.
Replication	All pigs received the same intervention, and there were no comparison groups or treatment conditions requiring allocation. The sample size in cell experimental groups were ≥ 3 to ensure replicability. From the measured results, the data showed high similarity within the same testing group, all attempts at replication were successful.
Randomization	Randomization was not applicable in this study, as it aimed to assess the technical feasibility and functional performance of a novel implantable system in a small number of animals. All animals underwent the same intervention, and no comparison groups or alternative treatment conditions were included that would necessitate allocation.
Blinding	Blinding was not performed, as the focus of this study was to verify the technical efficacy of a novel implantable cardiac pacemaker rather than to compare treatment groups based on a hypothesis. All procedures and outcomes were directly related to the assessment of device performance (e.g., output energy, pacing behavior), and therefore blinding would not have influenced data acquisition or interpretation, nor was it applicable to the study design.

Reporting for specific materials, systems and methods

We require information from authors about some types of materials, experimental systems and methods used in many studies. Here, indicate whether each material, system or method listed is relevant to your study. If you are not sure if a list item applies to your research, read the appropriate section before selecting a response.

Materials & experimental systems

n/a	Involved in the study
☐	☒ Antibodies
☐	☒ Eukaryotic cell lines
☒	☐ Palaeontology and archaeology
☐	☒ Animals and other organisms
☒	☐ Clinical data
☒	☐ Dual use research of concern
☒	☐ Plants

Methods

n/a	Involved in the study
☒	☐ ChIP-seq
☒	☐ Flow cytometry
☒	☐ MRI-based neuroimaging

Antibodies

Antibodies used	FITC-CD61 and PE-CD62P
Validation	FITC anti-mouse/rat CD61 Antibody (104305, BioLegend, 1:50), Application: FC; Verified Reactivity: Mouse, Rat PE anti-mouse/rat CD62P(P-selectin) Antibody (148305, BioLegend,1:100), Application: FC; Verified Reactivity: Mouse, Rat

Eukaryotic cell lines

Policy information about cell lines and Sex and Gender in Research

Cell line source(s)	The L929 cells were acquired from the Cell Bank of the Chinese Academy of Sciences in Beijing, China.
Authentication	No authentication as such was performed. However, at least three biological replicates were preformed for each donor cells to confirm the consistency of the cell lines.
Mycoplasma contamination	All cell lines were negative for mycoplasma.
Commonly misidentified lines (See ICLAC register)	No commonly misidentified lines were used in the work.

Animals and other research organisms

Policy information about studies involving animals; ARRIVE guidelines recommended for reporting animal research, and Sex and Gender in Research

Laboratory animals	Adult Yorkshire pigs (age: 1.5-2.0 years; weight: 68-89 kg; n=11) were acquired from State Key Laboratory of Cardiovascular Disease and Fuwai Hospital.
Wild animals	This study did not involve wild animals
Reporting on sex	Male(n=7) and Female(n=4)
Field-collected samples	This study did not involve samples collected from the field.
Ethics oversight	All experimental process was strictly in line with the institutional and national guidelines for the care and use of laboratory animals and the study protocol was reviewed and approved by the Ethical Committee of Animal Experimental Center in State Key Laboratory of Cardiovascular Disease and Fuwai Hospital (ethical approval number: 0104-1-4-ZX(X)-23).

Note that full information on the approval of the study protocol must also be provided in the manuscript.